Supplementary Information

The Paradox of Gold-Liposome Nanohybrids: The Location of Gold Enables Unconventional Properties and Drives Cellular Behavior

Ansuja P. Mathew,[1, 2, †] Vandhana Kandavelkumar,[1,2,†] Nabila Masud,[4] Sebastian Huerta-Romo Picazo,[5] Susheel Kumar Nethi,[1, 2] Saji Uthaman,[1,2,3] Xiaona Wen,[2] Wenyu Huang,[5 1, 2] Surya K. Mallapragada,[1, 2] Anwesha Sarkar,[4] Rizia Bardhan[1,2]*

[1]Department of Chemical and Biological Engineering, Iowa State University, Ames, Iowa, USA
[2]Nanovaccine Institute, Iowa State University, Ames, Iowa, USA
[3]Current address: Smart Materials and Devices (SMAD) Division, Yenepoya Research Centre, Yenepoya (Deemed to be University), Mangalore, 575018, India
[4]Department of Electrical and Computer Engineering, Iowa State University, Ames, Iowa, USA
[5]Department of Chemistry, Iowa State University, Ames, Iowa, USA

† These authors have contributed equally
***Corresponding author:** rbardhan@iastate.edu

Table of Contents

Page S3. Figure S1. Photothermal efficiency of GLNs developed with (a) DPPC/DSPE-PEG/DSPE-PEG-Amine liposomes and (b) DPPC/DSPE-PEG liposomes

Page S3. Figure S2. Physicochemical characterization of GLNs developed with DPPC/Chol liposomes and 0.1% and 0.3% of chitosan coating and representative TEM images of DPPC/Chol bare liposome and chitosan-coated liposome.

Page S4. Figure S3. Lower magnification TEM images of GLNs developed with DPPC/Chol liposomes and 0%, 0.001%, and 0.01% chitosan

Page S5 Figure S4. EDS analysis of 0% GLNs

Page S6 Figure S5. EDS analysis of 0.001% GLNs

Page S7 Figure S6. EDS analysis of 0.01% GLNs

Page S8. Figure S7. Physicochemical characterization DPPC/Chol liposome with different concentrations of 0.001%, 0.01%, 0.1%, and 0.3% of chitosan coating.

Page S8. Figure S8. Physicochemical characterization of DPPC/Chol/DSPE-PEG liposome with different concentrations of 0.001%, 0.01%, 0.1%, and 0.3% of chitosan coating.

Page S9. Figure S9. Physicochemical characterization of GLNs developed with DPPC/Chol/DSPE-PEG liposome with different concentrations of 0.001%, 0.01%, 0.1% and 0.3% of chitosan coating.

Page S10. Figure S10. Normalized Raman intensity of the liposome alone

Page S10. Figure S11. Thermogravimetry analysis of liposomes and GLNs

Page S11. Figure S12. *In vitro* stability of the GLNs 0%, 0.001% and 0.01%

Page S12. Figure S13: Contact mechanics model used to extract the Young's modulus from the force-indentation data, the Hertz model, and the Cone-Sphere model.

Page S13. Figure S14. Young's modulus measured for the different samples using the Hertz model

Page S13. Table S1. Young's modulus of bulk/metal NPs

Page S14. Table S2. Reference on cell studies done with NPs and substrate stiffness

Page S15. Table S3. Quantitative comparison of nanoparticle size and Young's Modulus estimations using Hertz and Cone-Sphere Contact Mechanics

Page S16. Figure S15. *In vitro* cellular viability of finalized GLNs developed with DPPC/ cholesterol liposomes with (0.001% and 0.01%) or without chitosan (0%) in DC 2.4 and MODE-K cells.

Page S17. Figure S16. *In vitro* cell uptake of different concentrations of finalized GLNs developed with DPPC/cholesterol liposomes and 0.001% chitosan. in DC2.4 and MODE-K cells.

Page S17. Figure S17. *In vitro* cell uptake of finalized GLNs developed with DPPC/cholesterol liposomes with (0.001% and 0.01%) or without chitosan (0%) in DC 2.4 and MODE-K cells

Page S18. Figure S18. *In vitro* cell uptake of different GLNs at different time points from 1h to 24h in (a) DC2.4 cells and (b) MODE-K cells validated using ICP-MS analysis.

Page S19. Figure S19. *In vitro* cell viability performed after treating DC2.4 and MODE-K cells with different inhibitors. Representative overlay images of (c) DC2.4 and (d) MODE-K cells incubated with GLNs for 6 h with and without pre-treatment with genistein.

Page S20. Figure S20. a) Representative images of MODE-K and DC2.4 cells from live/dead assay

Page S21. Figure S21. a) Quantification of the different functional parameters for glycolysis from ECAR curves: a) glycolysis and b) glycolytic reserve.

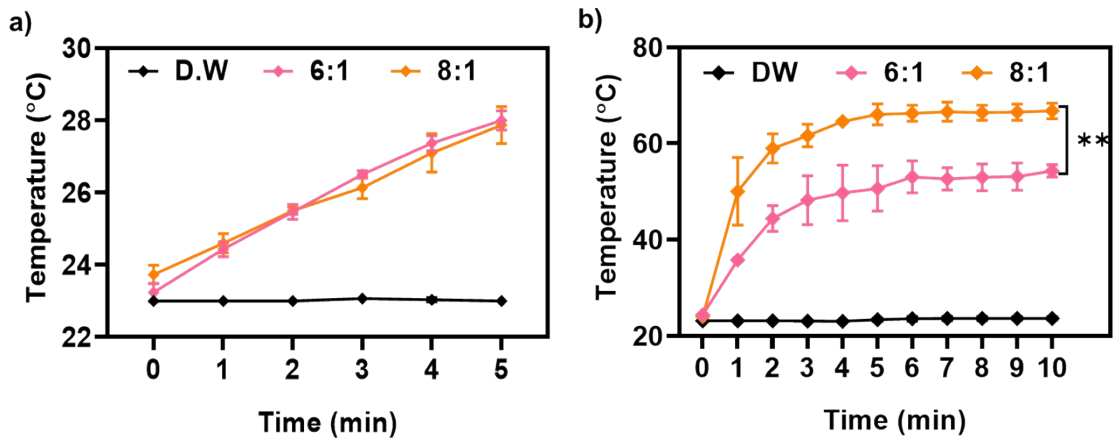

Figure S1: Photothermal efficiency of Gold-liposome nanoparticles developed with (a) DPPC/DSPE-PEG/DSPE-PEG-Amine liposomes and (b) DPPC/DSPE-PEG liposomes with two different ascorbic acid: gold chloride (AA: Au) ratios.

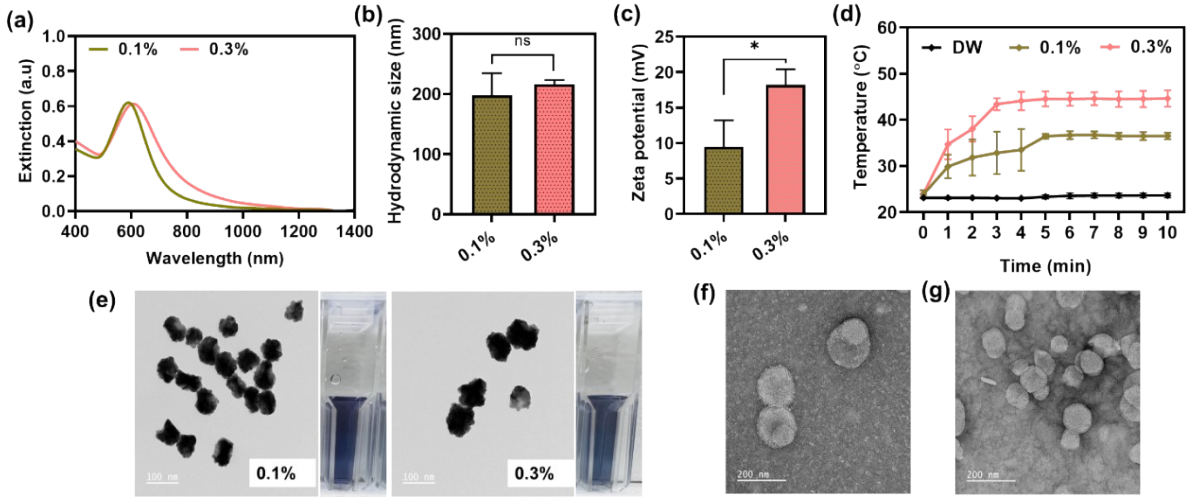

Figure S2. Physicochemical characterization of Gold-liposomes nanohybrids developed with DPPC/Chol liposomes and higher concentrations (0.1% and 0.3%) of chitosan coating and 8:1 ascorbic acid to gold chloride ratio. (a) UV-Vis spectroscopy, (b) Hydrodynamic size, (c) Zeta potential and (d) Photothermal efficiency, and (e,f) TEM analysis (inset: Optical image of the sample in cuvettes) scale bar = 100 nm. Representative TEM images of (f) DPPC/Chol bare liposome and (g) chitosan-coated liposome. Scalebar=200 nm.

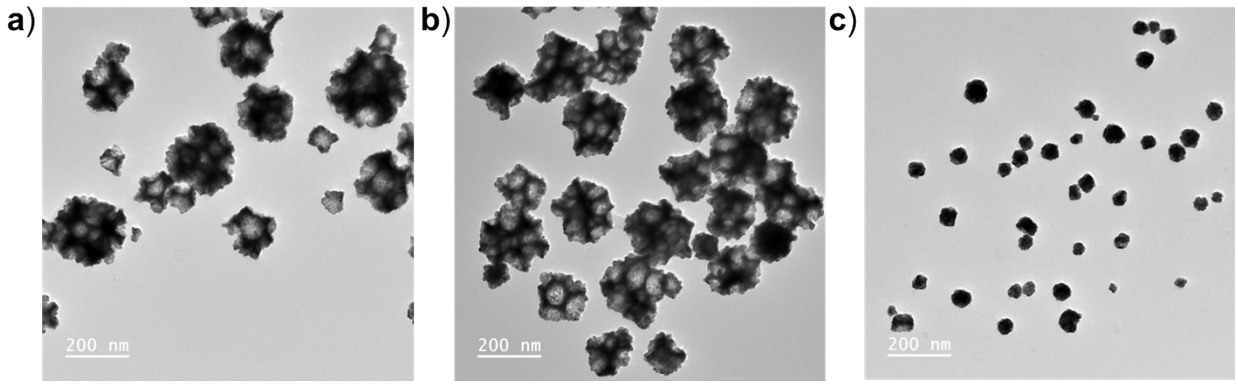

Figure S3: Lower magnification TEM images of Gold-liposomes nanohybrids developed with DPPC/Chol liposomes and (a) 0%, (b) 0.001%, and (c) 0.01% chitosan and 8:1 ascorbic acid to gold chloride ratio. Scale bar =200nm in all images.

Figure S4. EDS analysis of 0% GLNs (a) low magnification and (b) high magnification TEM images along with EDS spectrum (region 1 corresponding to the GLNs and region 2 corresponding to the empty grid), and elemental mapping showing distribution of Au on GLNs.

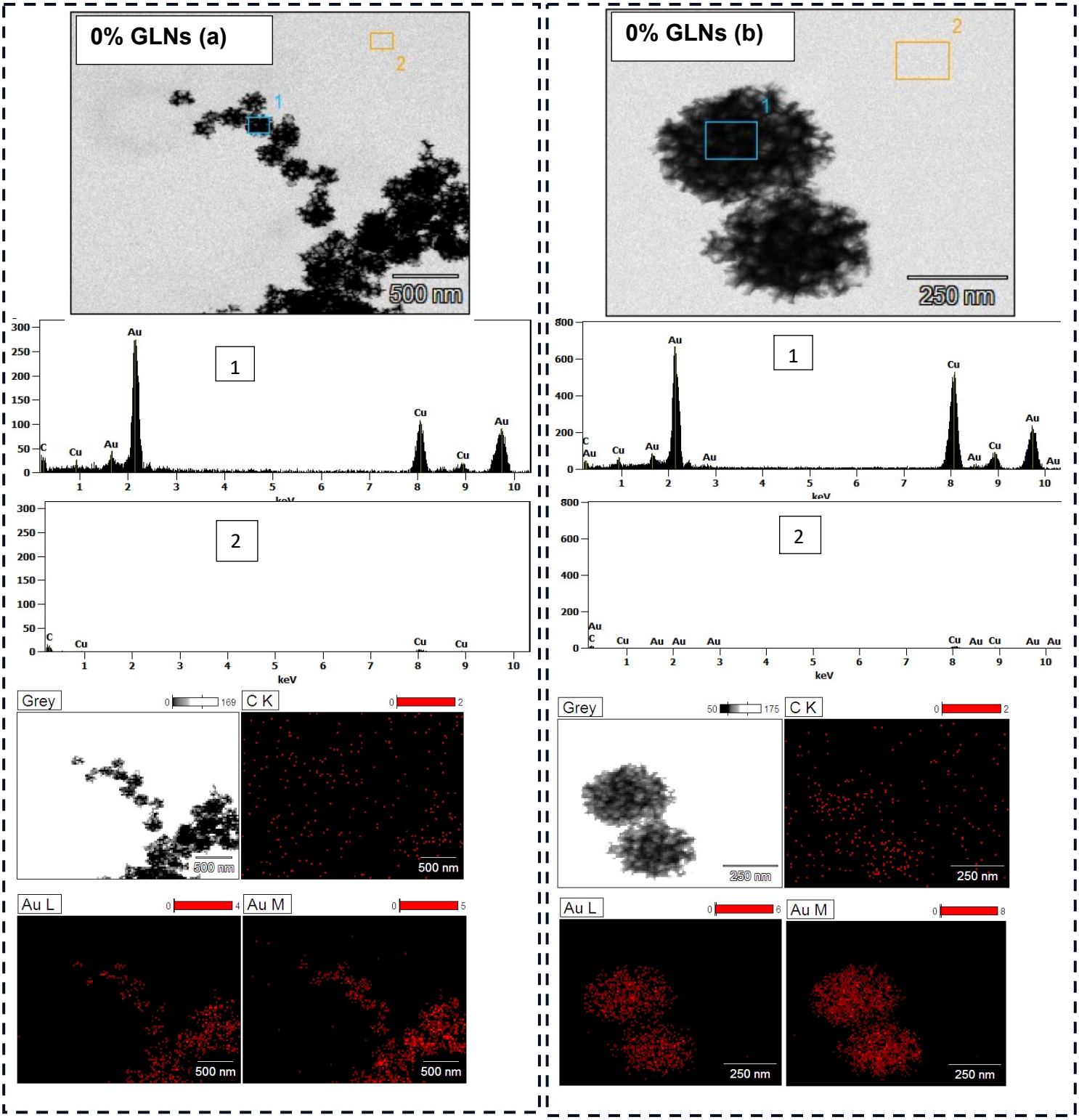
0% GLNs (a)
0% GLNs (b)
500 nm
250 nm
1
2
keV
Grey
C K
Au L
Au M

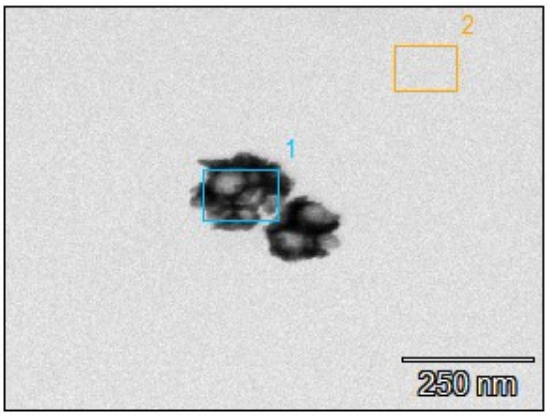

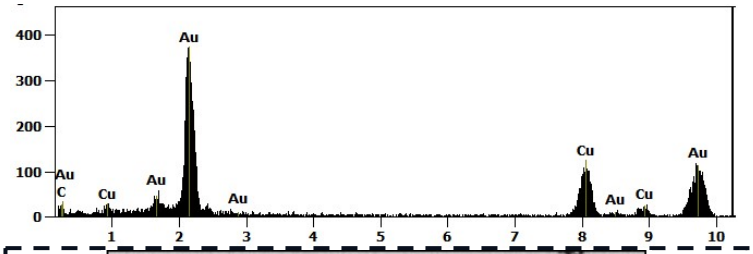

0.001% GLNs (a)

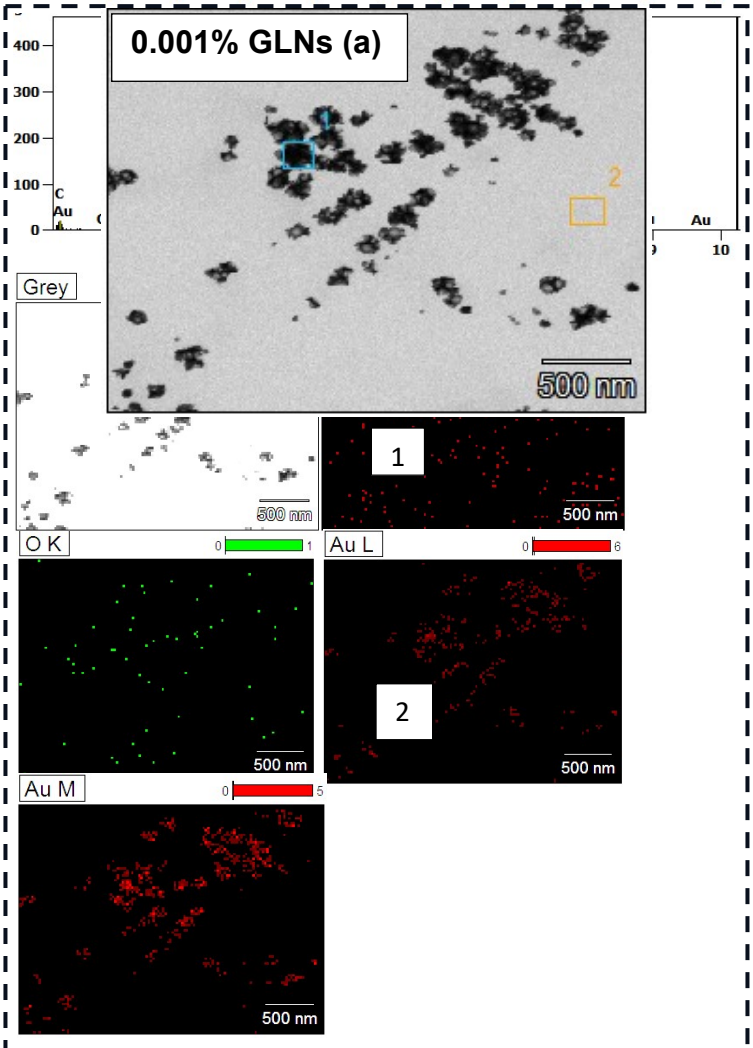

0.001% GLNs (b)

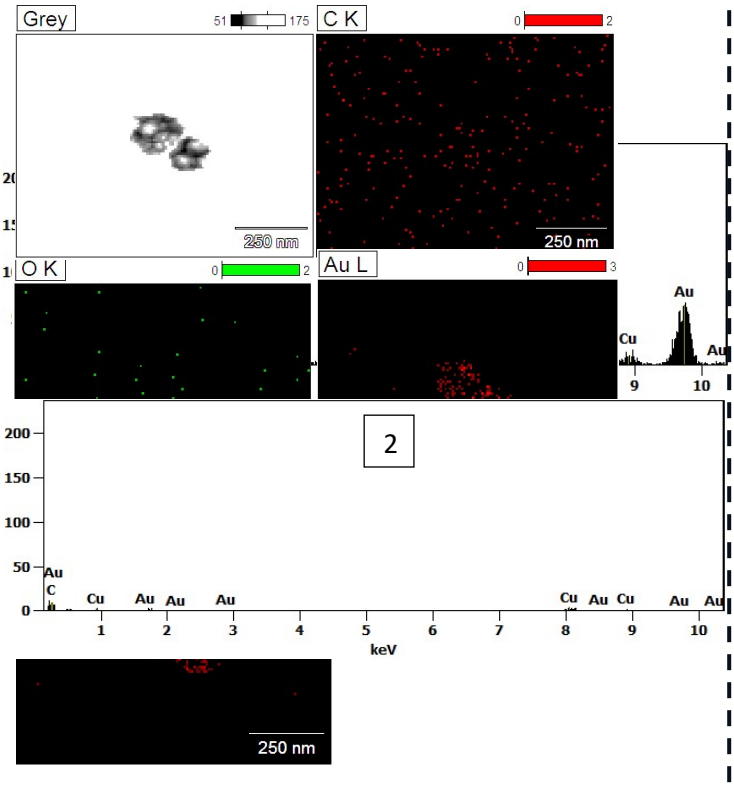

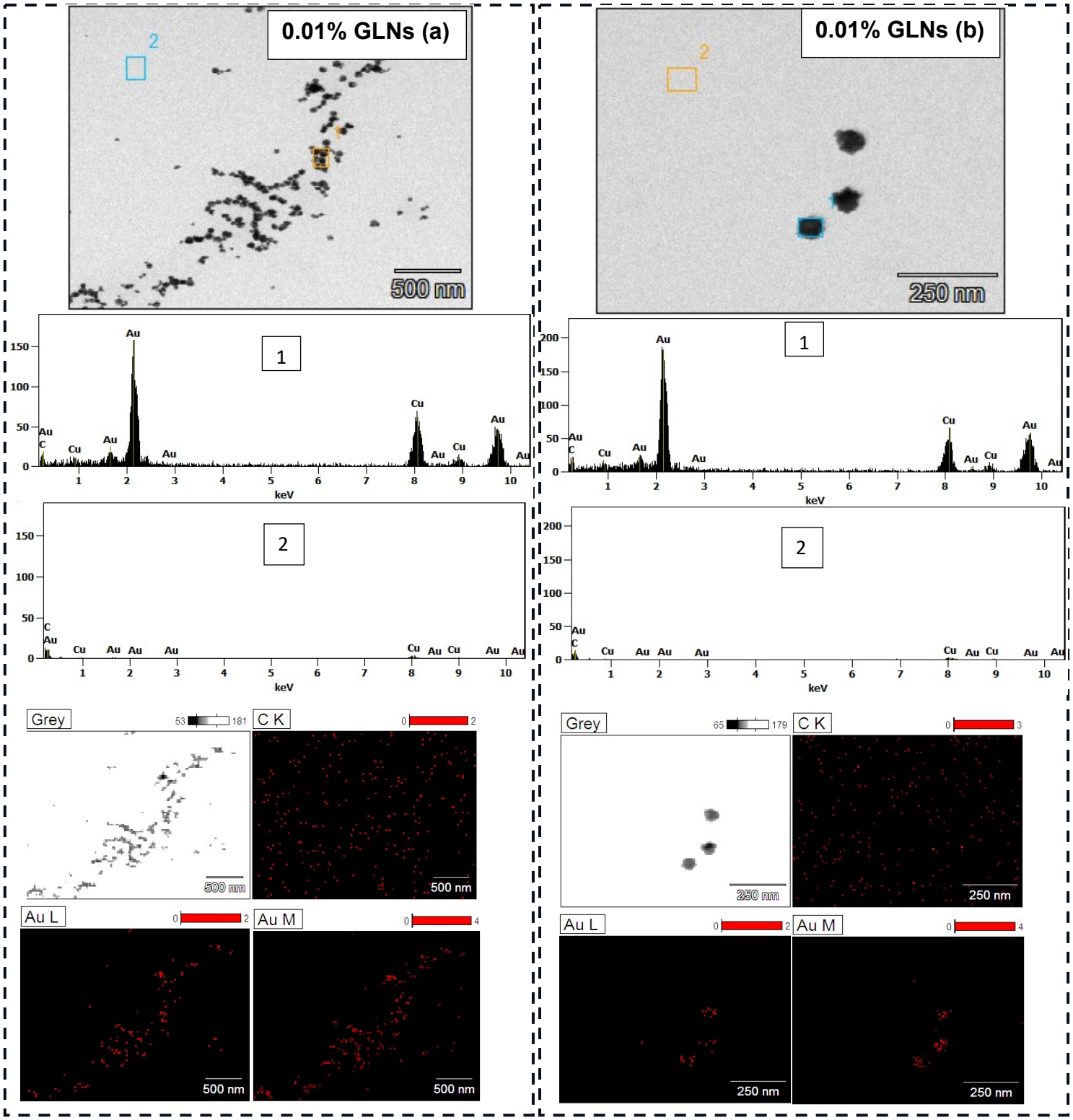

Figure S5.EDS analysis of 0.001% GLNs (a)low magnification and (b) high magnification TEM images along with EDS spectrum (region 1 corresponding to the GLNs and region 2 corresponding to the empty grid), and elemental mapping showing distribution of Au on GLNs.

Figure S6.EDS analysis of 0.01% GLNs (a)low magnification and (b) high magnification TEM images along with EDS spectrum (region 1 corresponding to the GLNs and region 2 corresponding to the empty grid), and elemental mapping showing distribution of Au on GLNs.

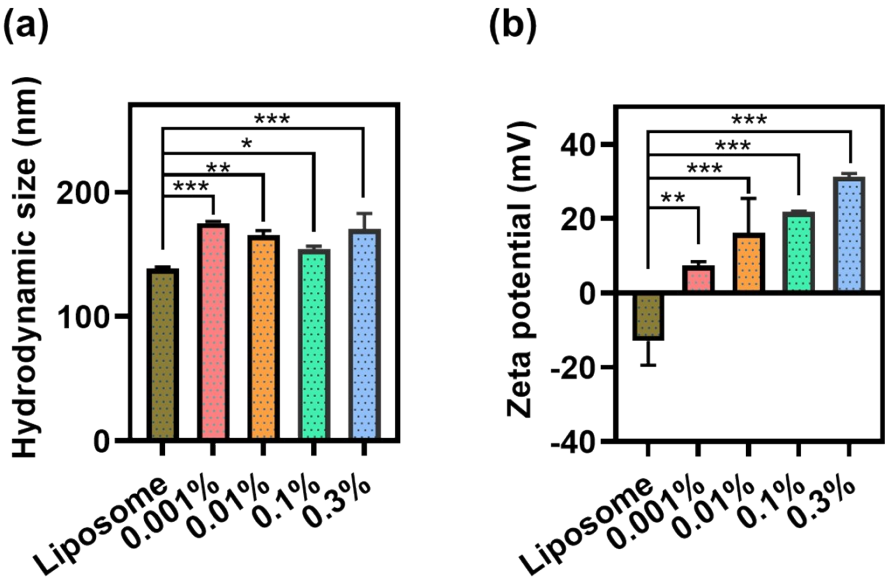

Figure S7. Physicochemical characterization DPPC/Chol liposome with different concentrations (0.001%, 0.01%, 0.1%, and 0.3%) of chitosan coating. (a) Hydrodynamic size (b) Zeta potential

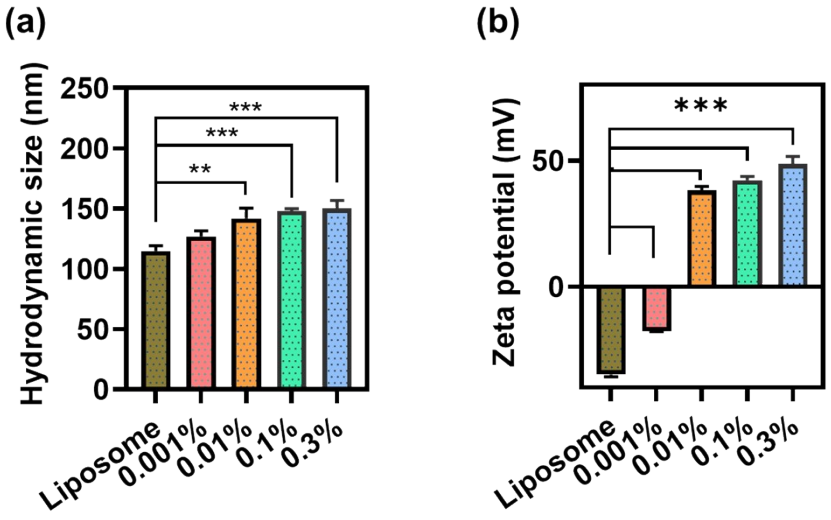

Figure S8. Physicochemical characterization DPPC/Chol/DSPE-PEG liposome with different concentrations of 0.001%, 0.01%, 0.1% and 0.3% of chitosan coating. (a) Hydrodynamic size (b) Zeta potential

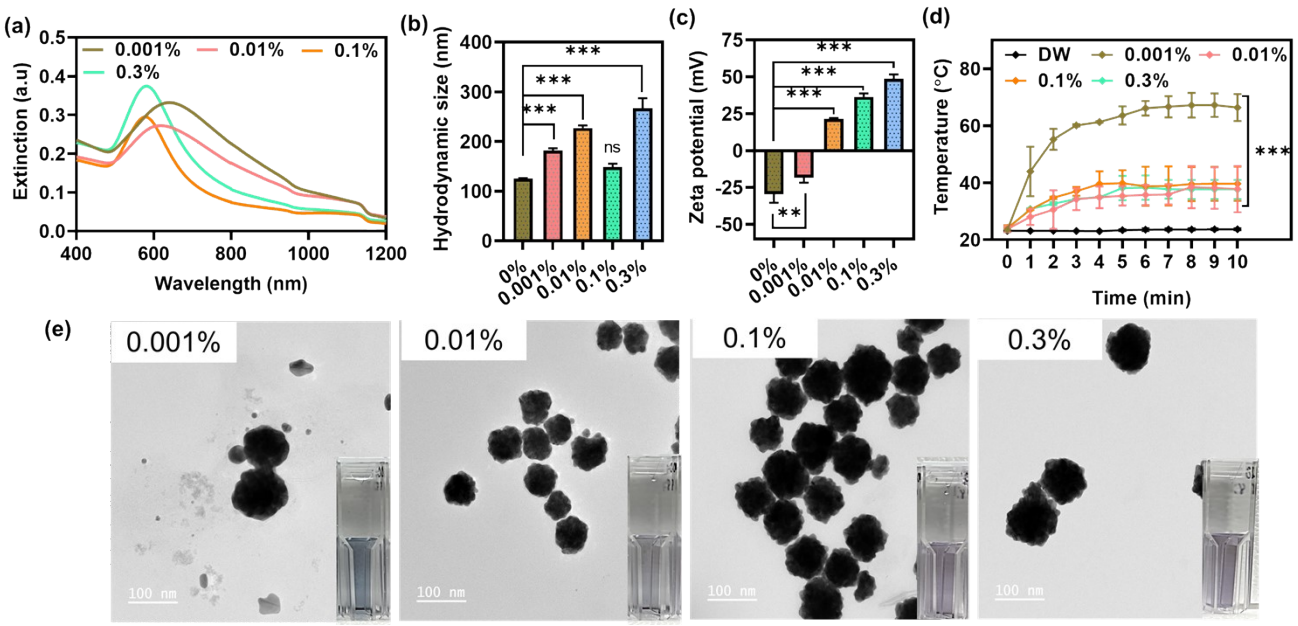

Figure S9. Physicochemical characterization of GLNs developed with DPPC/Chol/DSPE-PEG liposome with different concentrations of 0.001%, 0.01%, 0.1% and 0.3% of chitosan coating and 8:1 ascorbic acid to gold chloride ratio. (a) UV-Vis spectroscopy (b) Hydrodynamic size, (c) Zeta potential, (d) Photothermal efficiency, and (e) TEM analysis (inset: Optical image of the sample in cuvettes), (scale bar = 100 nm).

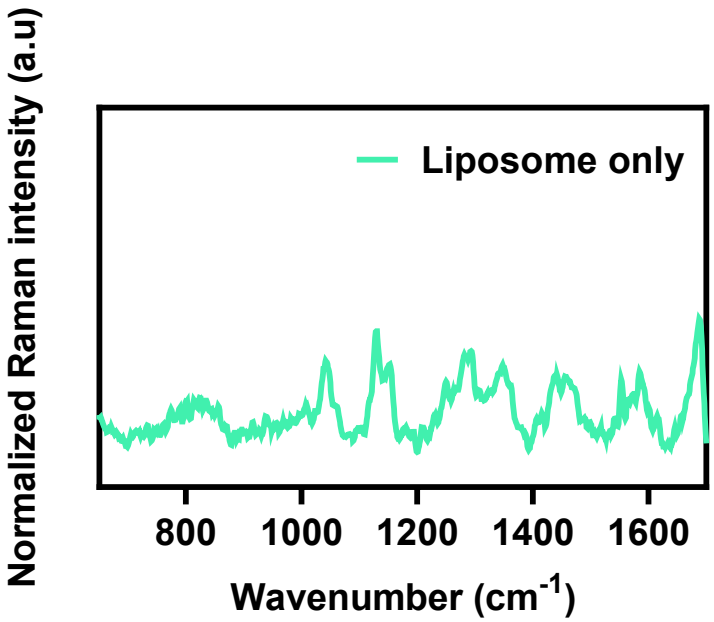

Figure S10. Normalized Raman intensity of liposome alone

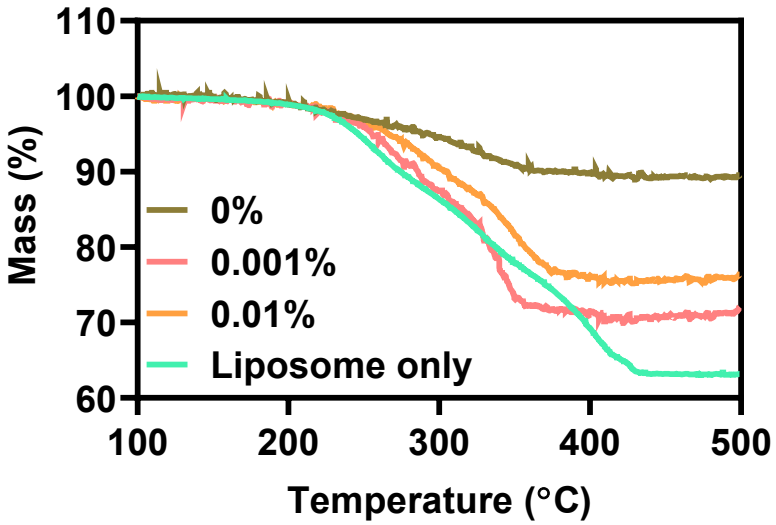

Figure S11. Thermogravimetry analysis of liposomes and GLNs

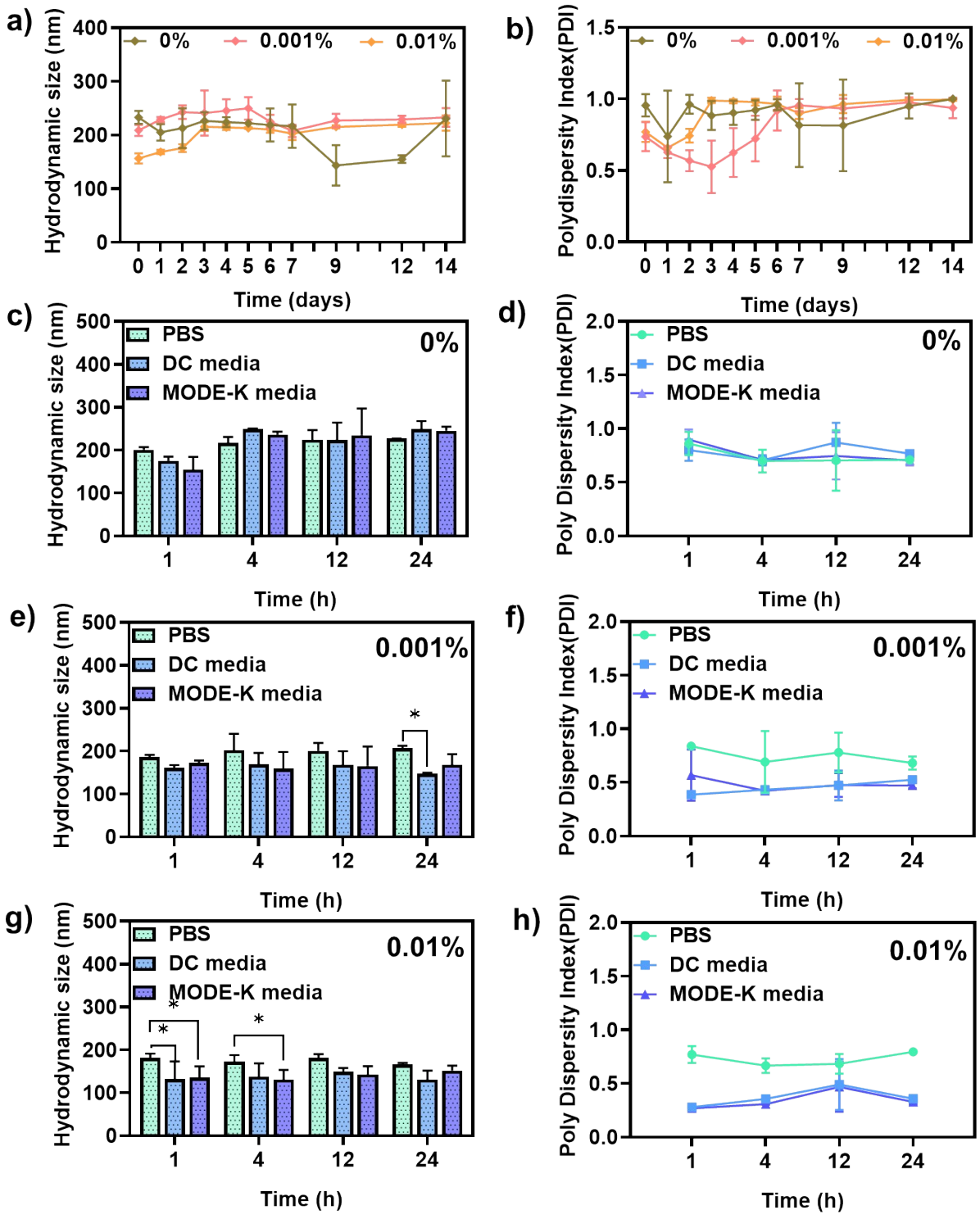

Figure S12. *In vitro* stability of the GLNs 0%, 0.001% and 0.01% showing hydrodynamic diameter and polydispersity index (PDI), (a-b) in Milli-Q water for up to 14 days (c-h) in PBS, and culture media used for the cell uptake studies for up to 24 h.

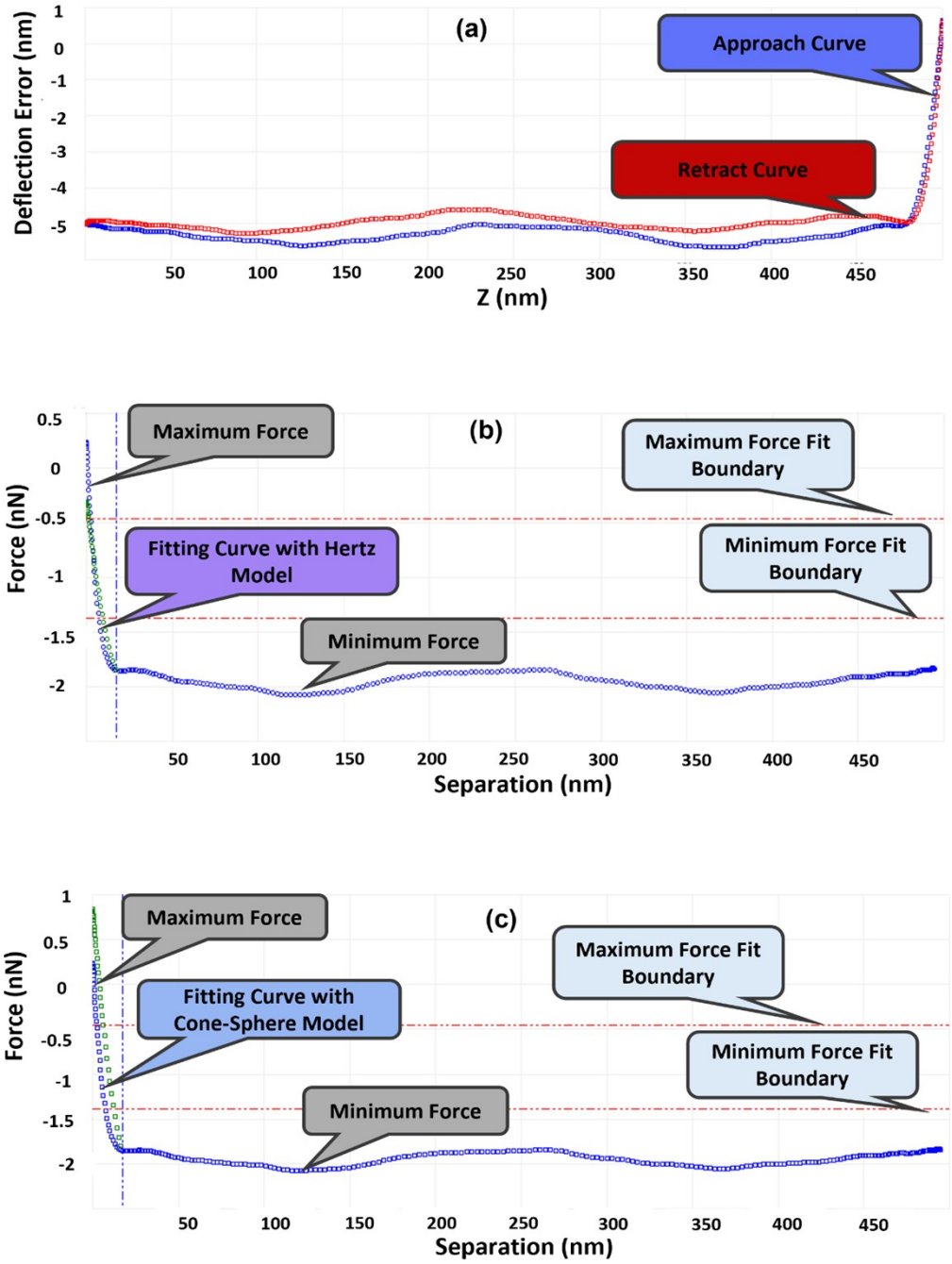

Figure S13. (a) Deflection error vs Z curves obtained during Peak Force QNM measurements, representing the approach (blue) and retract (red) curves. The approached curve was fitted and the fitted region using the (b) Hertz or (c) Cone-Sphere model is shown by the green curve that is superimposed with the raw data. Retraction was not utilized in the modulus computation, represented by the red curve. The indentation depth was kept within the bounds between maximum and minimum force fit boundary (red dotted lines) where the model assumptions hold by fitting in the approach curve's elastic regime.

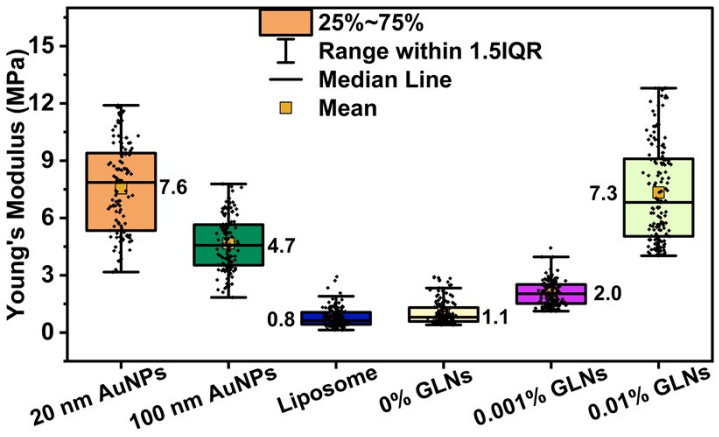

Figure S14. Young's modulus measured for the different samples using the Hertz model

Table S1. Young's modulus of bulk/metal NPs

	Metal /modified metal nanoparticle	Young's modulus	Model used	Ref
1	Gold Nanostars on PDMS	200 MPa	Derjaguin-Muller-Toporov (DMT) model	[1]
2	Pristine GNPs	32.69 ± 6.57 MPa	Derjaguin-Muller-Toporov (DMT) model	[2]
3	Peptide modified GNPs	10.66 ± 1.75 MPa	Derjaguin-Muller-Toporov (DMT) model	[2]
4	AuNP doped hydrogel	2.7 MPa		[3]
5	Aerogels with AgNPs	83.9 MPa		[3]
6	Gold nanoparticle- decorated polyethylene glycol- hydroxyapatite (PEG-AuNP)	6 MPa		[4]
7	AuNPs > 6nm	60 GPa (elastic modulus)	Hertzian model	[5]
8	Nanodimensional metallic silver	103.93 GPa (elastic modulus)		[6]
9	Copper Alloys - Nickel Silvers	120-140 GPa		[7]

Table S2. Reference on cell studies done with NPs and substrate stiffness

	Nanoparticle uptaken by cells	Young's Modulus	Model used	Ref
1	DSPC:DSPG liposome (molar ratio 4:1)	3.6±1.2 Mpa	Hertz/Sneddon model	[8]
2	DSPC:DSPG:CHOL (molar ratio 4:1:2)	1.4±0.5 MPa	Hertz/Sneddon model	[8]
3	Nanolipogels with alginate core	0.036- 24 MPa	-	[9]
4	Phospholipid liposomes	45 kPa- 53.3 MPa	-	[10]
5	PLGA core lipid shell nanoparticles	5 MPa- 110 Mpa	-	[11]
6	PEG hydrogel nanoparticles	0.01-3 MPa	-	[12]
7	Zwitterionic nanoparticle with carboxybetaine dimethacrylate and carboxybetaine methacrylate	4.4- 165 MPa	-	[13]
8	Silica nanocapsules	0.7 MPa	Hertzian contact model	[14]
9	Hydrogel nanoparticles	0.37-3.15 MPa	-	[15]
10	Gelatin nanoparticles	5.48-14.26 MPa	Hertz model	[16]
	Substrates for cell growth	**Young's Modulus**	**Model used**	**Ref**
11	Polydimethylsiloxane (PDMS)	5kPa-1.72 MPa	-	[17]
12	Polyacrylamine (PAA) hydrogel	7.2-37 kPa	-	[18]
13	PDMS	1.8-0.2 MPa	-	[18]
15	PDMS	10-1500 KPa	-	[19]
16	Polyvinyl alcohol	4.5-37 kPa	-	[20]
17	PAA-PAH films	150 MPa	Hertz model	[21]
18	Silica layer on PDMS	7 MPa	Hertzian model	[22]

Table S3. Quantitative comparison of nanoparticle size, roughness, and Young's Modulus estimations using Hertz and Cone-Sphere Contact Mechanics

Nanoparticles (NPs)	Size (nm) (Mean ± SD)	Roughness (nm) (Mean ± SD)	Young's Modulus (MPa) Hertzian Model (Mean ± SD)	Young's Modulus (MPa)- Cone-Sphere Model (Mean ± SD)
20 nm AuNPs	51.2 ± 6.28	1.8 ± 0.3	7.54 ± 2.32	46.3 ± 6.75
100 nm AuNPs	145.4 ± 16.2	3.4 ± 0.9	4.76 ± 1.38	39.2 ± 7.17
Liposome	114.0 ± 10.7	1.8 ± 0.5	0.79± 0.48	4.01± 0.98
0% GLNs	167.9 ± 14.8	2.2 ± 0.7	1.04 ± 0.64	11.5 ± 2.27
0.001% GLNs	200.7 ± 12.1	2.7 ± 0.7	2.05 ± 0.63	19.3 ± 2.28
0.01% GLNs	156.8 ± 16.4	3.2 ± 0.9	7.33 ± 2.55	50.5 ± 4.99

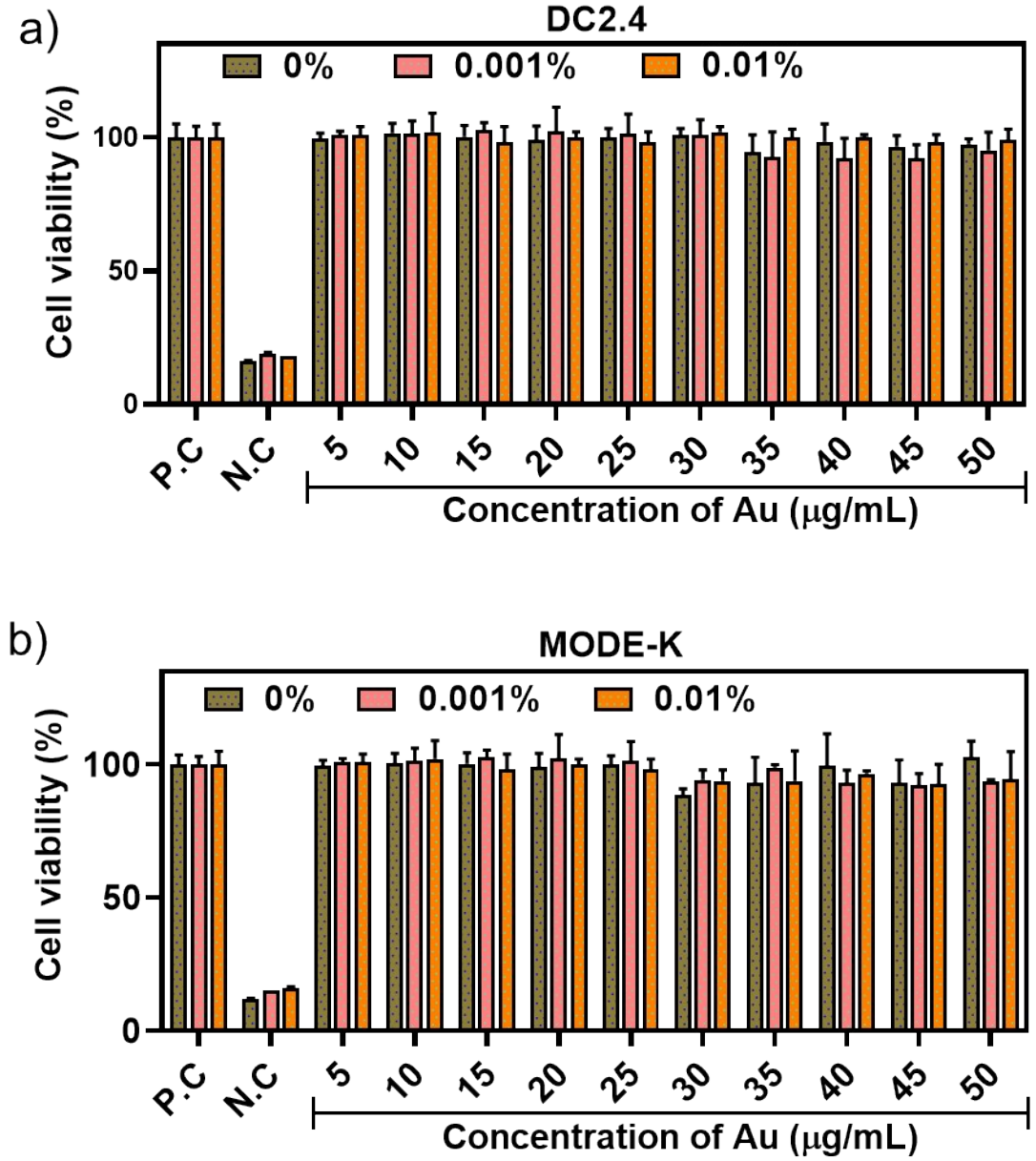

Figure S15. *In vitro* cellular viability of finalized Gold-liposome nanohybrids developed with DPPC/cholesterol liposomes without chitosan (0%), DPPC/cholesterol liposomes with 0.001% chitosan, and DPPC/cholesterol liposomes with 0.01% chitosan. (a) DC 2.4 and (b) MODE-K cells. P.C. represents cells alone, and N.C represents cells treated with 0.1% Triton-X 100.

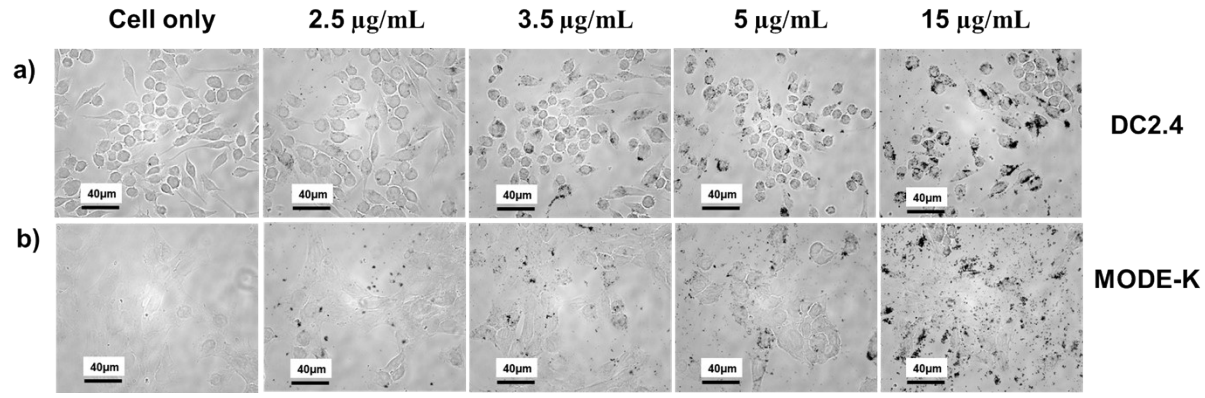

Figure S16. Representative images showing cellular uptake of different concentrations of DPPC/cholesterol liposomes with 0.001% chitosan obtained after 6 h incubation in (a) DC2.4 and (b) MODE-K cells. Scalebar=40µm

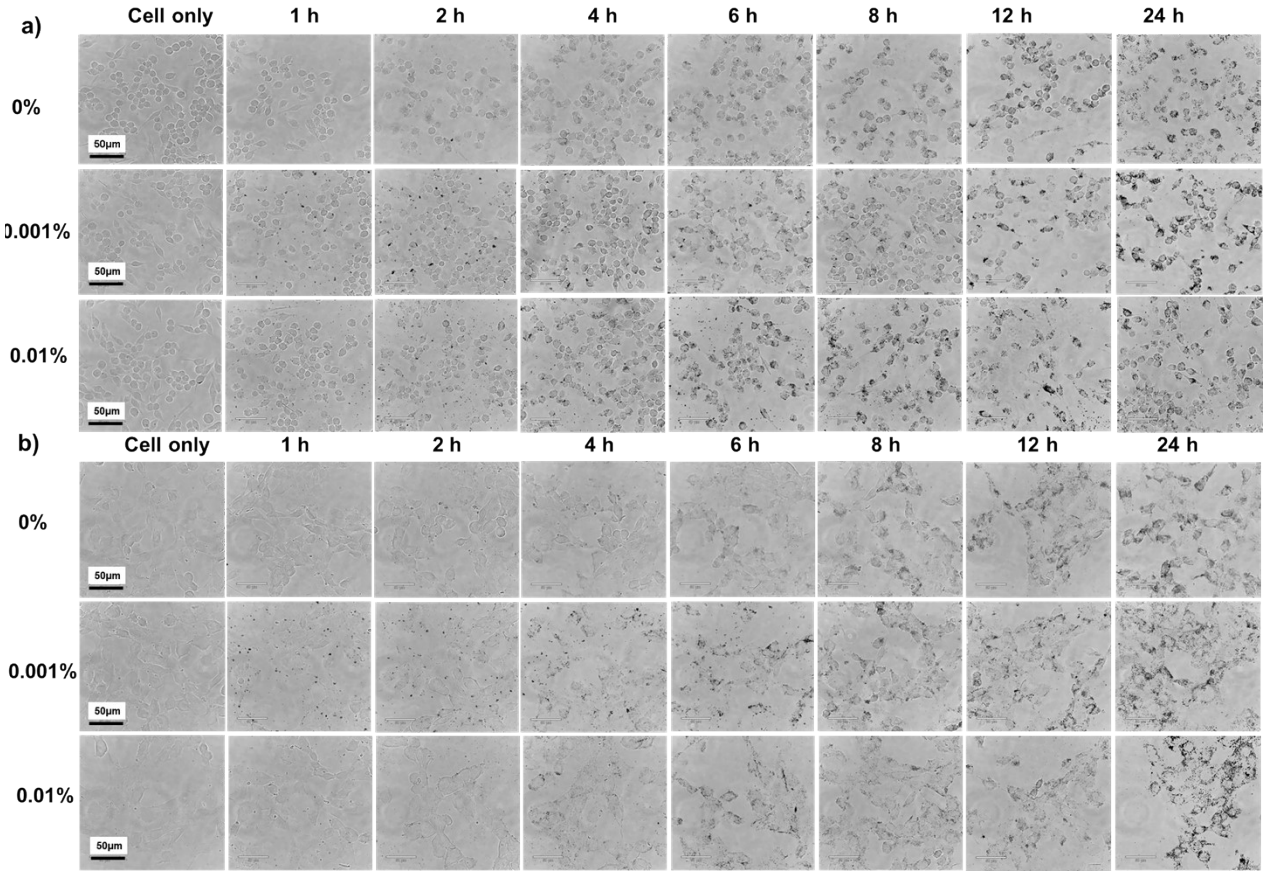

Figure S17. *In vitro* cell uptake of finalized Gold-liposome nanohybrids developed with DPPC/cholesterol liposomes without chitosan (0%), DPPC/cholesterol liposomes with 0.001% chitosan and DPPC/cholesterol liposomes with 0.01% chitosan. Representative images showing cellular uptake at different time points from 1h to 24h in (a) DC2.4 cells and (b) MODE-K cells. Scalebar=50µm.

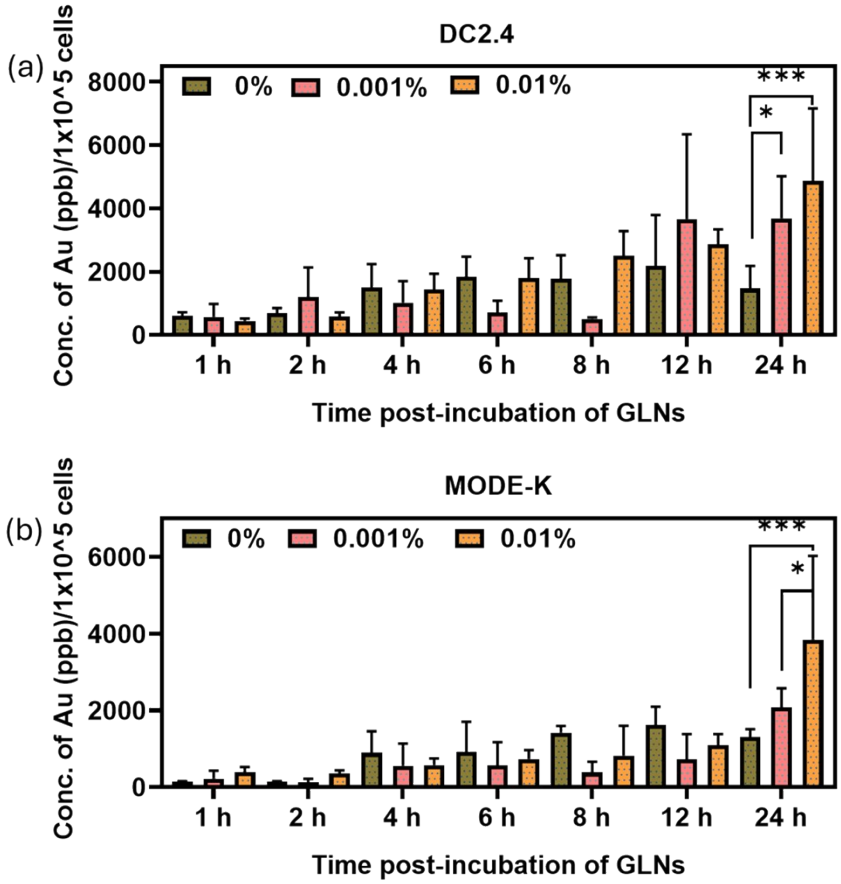

Figure S18. *In vitro* cell uptake of different GLNs at different time points from 1h to 24h in (a) DC2.4 cells and (b) MODE-K cells validated using ICP-MS analysis

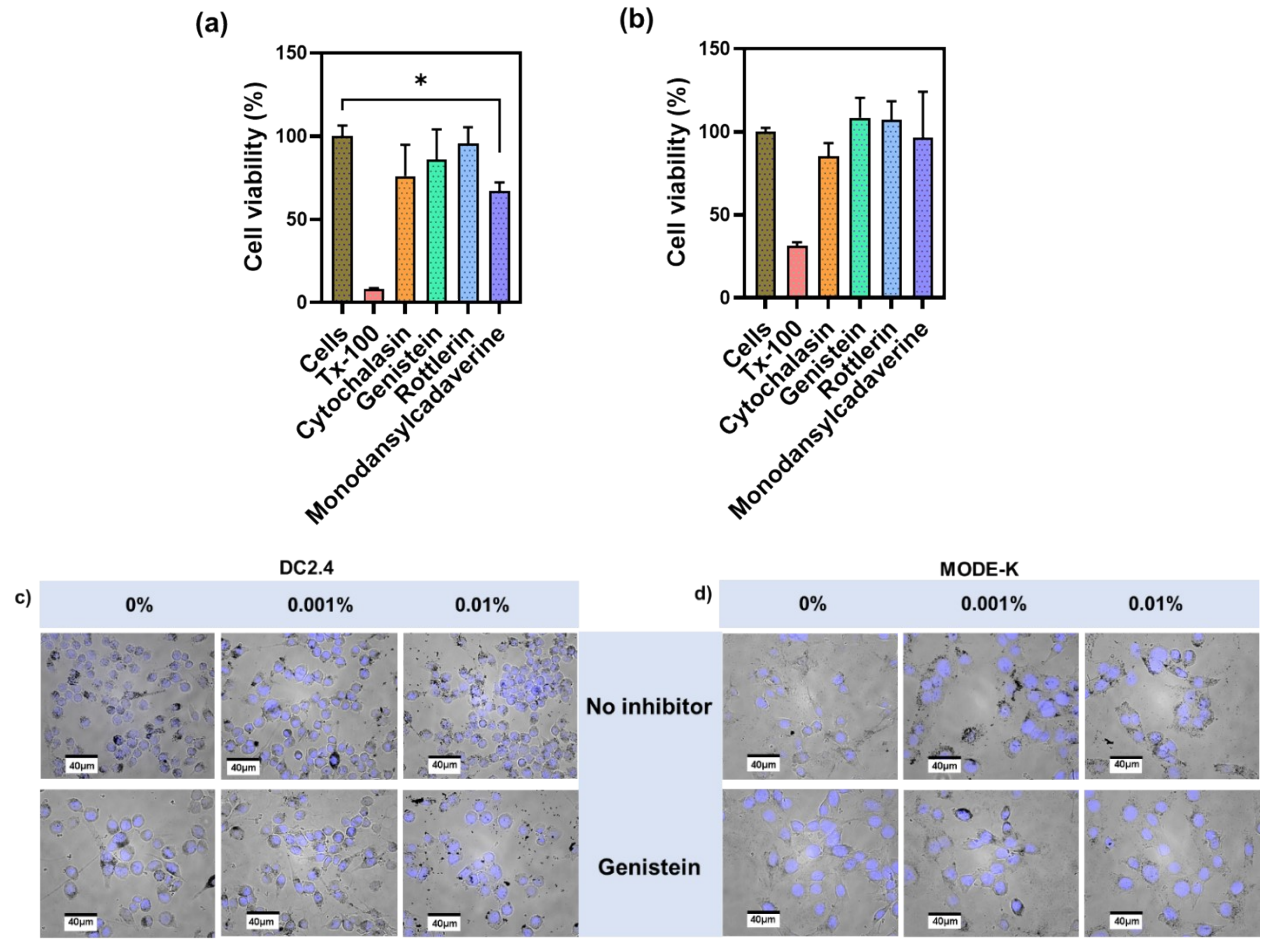

Figure S19. *In vitro* cell viability performed after treating (a) DC2.4 and (b) MODE-K cells with different inhibitors. Representative overlay images of brightfield and DAPI (blue) in (c) DC2.4 and (d) MODE-K cells incubated with GLNs synthesized without chitosan (0%), with 0.001% chitosan and with 0.01% chitosan for 6 h with and without pre-treatment with inhibitor (genistein). Scale bar=40µm. Here genistein inhibits caveolae-mediated endocytosis.

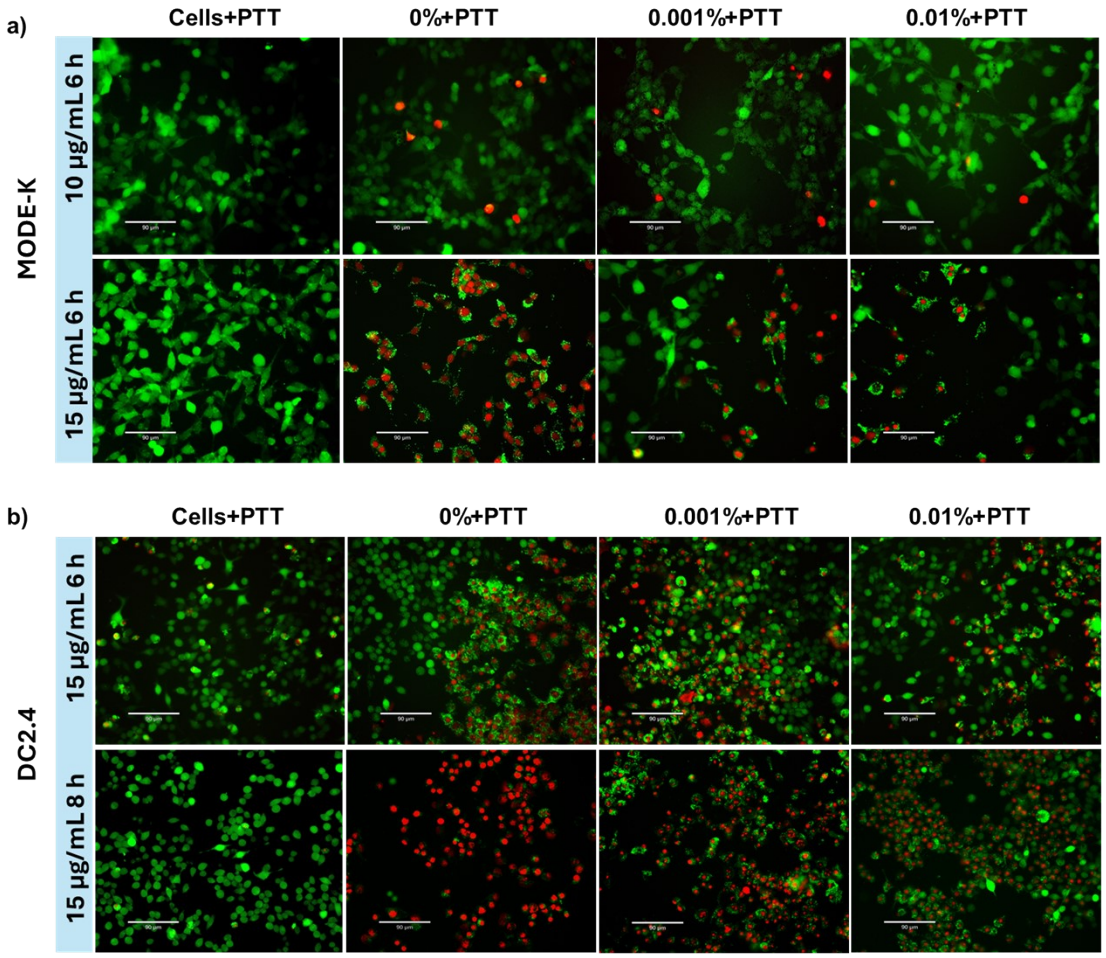

Figure S20. a) Representative images of MODE-K cells stained with calcein/PI after incubation of 10 µg/mL and 15 µg/mL GLNs for 6h followed by laser irradiation b) Representative images of DC2.4 cells stained with calcein/PI after incubation of 15 µg/mL GLNs for 6h and 8h. Scale bar=90 µm.

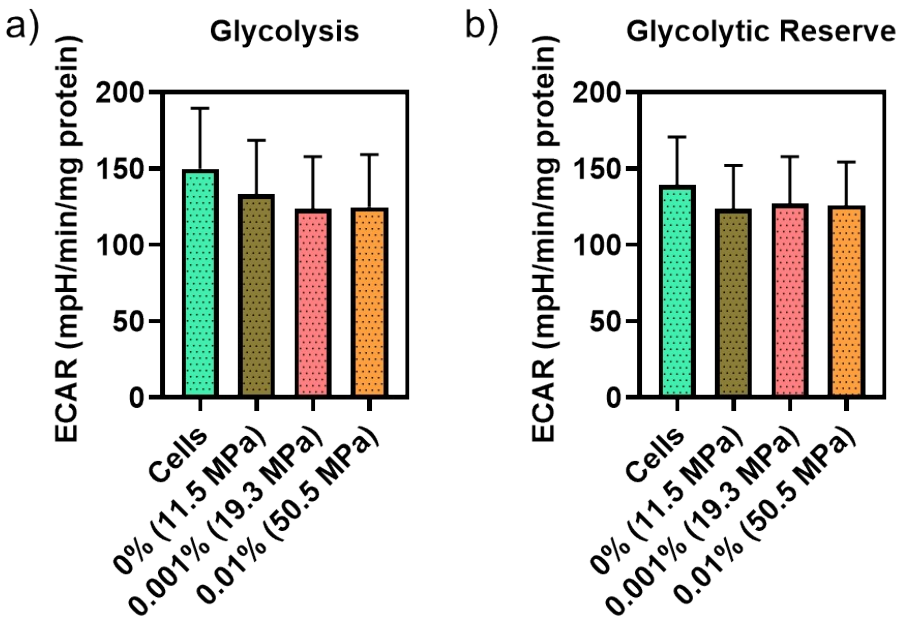

Figure S21. a) Quantification of the different functional parameters for glycolysis from ECAR curves a) glycolysis and b) glycolytic reserve.

References

1. P. Knittel, O. Bibikova and C. Kranz, *Faraday Discussions*, 2016, **193**, 353-369.
2. T. Kulkarni, D. Mukhopadhyay and S. Bhattacharya, *Applied Surface Science*, 2022, **591**, 153175.
3. S. E. Turk, D. Chekkaramkodi, M. Ali, A. A. Sajini and H. Butt, *Materials & Design*, 2025, **250**, 113650.
4. C. C. Shen, S. H. Hsu, K. B. Chang, C. A. Yeh, H. C. Chang, C. M. Tang, Y. C. Yang, H. H. Hsieh and H. S. Hung, *Biomedicines*, 2021, **9**.
5. H. Li, Y. Han, T. Duan and K. Leifer, *Applied Physics Letters*, 2019, **115**.
6. D. R. Saha, A. Mandal, S. Mitra, M. R. Mada, P. Boughton, S. Bandyopadhyay and D. Chakravorty, *AIP Conference Proceedings*, 2013, **1536**, 257-258.
7. A. materials, *Copper Alloys - Nickel Silvers*, 2001.
8. N. Benne, R. J. T. Leboux, M. Glandrup, J. van Duijn, F. Lozano Vigario, M. A. Neustrup, S. Romeijn, F. Galli, J. Kuiper, W. Jiskoot and B. Slütter, *Journal of Controlled Release*, 2020, **318**, 246-255.
9. P. Guo, D. Liu, K. Subramanyam, B. Wang, J. Yang, J. Huang, D. T. Auguste and M. A. Moses, *Nature communications*, 2018, **9**, 130.
10. Z. Dai, M. Yu, X. Yi, Z. Wu, F. Tian, Y. Miao, W. Song, S. He, E. Ahmad, S. Guo, C. Zhu, X. Zhang, Y. Li, X. Shi, R. Wang and Y. Gan, *ACS nano*, 2019, **13**, 7676-7689.
11. M. Yu, L. Xu, F. Tian, Q. Su, N. Zheng, Y. Yang, J. Wang, A. Wang, C. Zhu, S. Guo, X. Zhang, Y. Gan, X. Shi and H. Gao, *Nature communications*, 2018, **9**, 2607.

12. A. C. Anselmo, M. Zhang, S. Kumar, D. R. Vogus, S. Menegatti, M. E. Helgeson and S. Mitragotri, *ACS nano*, 2015, **9**, 3169-3177.
13. Y. Zheng, L. Xing, L. Chen, R. Zhou, J. Wu, X. Zhu, L. Li, Y. Xiang, R. Wu, L. Zhang and Y. Huang, *Biomaterials*, 2020, **262**, 120323.
14. Y. Hui, D. Wibowo, Y. Liu, R. Ran, H.-F. Wang, A. Seth, A. P. J. Middelberg and C.-X. Zhao, *ACS nano*, 2018, **12**, 2846-2857.
15. X. Chen, S. Zhang, J. Li, X. Huang, H. Ye, X. Qiao, Z. Xue, W. Yang and T. Wang, *Advanced science (Weinheim, Baden-Wurttemberg, Germany)*, 2022, **9**, e2202644.
16. A. V. Weiss, D. Schorr, J. K. Metz, M. Yildirim, S. A. Khan and M. Schneider, *Beilstein journal of nanotechnology*, 2022, **13**, 778-787.
17. R. N. Palchesko, L. Zhang, Y. Sun and A. W. Feinberg, *PloS one*, 2012, **7**, e51499.
18. A. M. Smith, D. G. Inocencio, B. M. Pardi, A. Gopinath and R. C. Andresen Eguiluz, *ACS Applied Polymer Materials*, 2024, **6**, 2405-2416.
19. S. Masterton and M. Ahearne, *Royal Society open science*, 2019, **6**, 191796.
20. T. Xia, R. Zhao, W. Liu, Q. Huang, P. Chen, Y. N. Waju, M. K. Al-Ani, Y. Lv and L. Yang, *Journal of cellular physiology*, 2018, **233**, 6996-7006.
21. A. Schneider, G. Francius, R. Obeid, P. Schwinté, J. Hemmerlé, B. Frisch, P. Schaaf, J. C. Voegel, B. Senger and C. Picart, *Langmuir : the ACS journal of surfaces and colloids*, 2006, **22**, 1193-1200.
22. J. Li, D. Han and Y.-P. Zhao, *Scientific Reports*, 2014, **4**, 3910.